We thank all the reviewers for spending their valuable time to review our manuscdript. We are also happy to receive constructive comments of the reviewers and please check our reponses to your valuable comments below.

Reply to reviewer 1

Technical Points:

1. With various z definitions, and d_0 and d_t, it is easy to be confused about what reference height is being used. The authors should try to ensure consistency, such as when z is referenced and then d_t is introduced. Is z still relative to d_0 in that case when seen in later equations such as (4)-(5)?

Reply: As the reviewer pointed out, the coordinate systems between the original surface layer scheme and the RSL scheme proposed by Harman and Finnigan are different. For better understanding of these two different vertical coordinates, we added a figure to show differences of the two vertical coordinates. Please consider that we did coordinate transform from the RSL theory to the WRF surface layer scheme to couple the RSL model into the WRF. That is, z is defined as the distance from the conventional zero-plane displacement height (d_0) and therefore, $d_t(= h - d_0)$, distance between d_0 and canopy height (h) is matched to z at canopy top ($z = d_t$). For better clarification of this point, we revised our manuscript with additional schematic diagram.

2. Eq. (2). Using an infinite upper bound implies that the length scale in (3) is still below the lowest model level? If so, this needs to be made clear because it is not obvious what length scale (3) has.

Reply: About this issue, we want to cite the paragraph in Harman and Finnigan (2007): "the infinite upper bound in (3) indicates that the mixing layer eddies originate at the canopy top hence their influence on the wind speed profile should decrease with increasing height. Therefore the $z \to \infty$ limits of the wind speed profile with and without the roughness sublayer influence ($\hat{\phi}_c \equiv 1$) are equal." Accordingly, the upper bound is not related to the lowest model level and we revised our manuscript for better readability.

3. Eq. (4). This introduces f and does not define it as far as I can tell.

Reply: As the reviewer suggested, we added the definition of f in Appendix A, list of symbols and definitions.

4. The positions of d_0, d_t and h relative to each other may be helpful to visualize with a schematic, along with how z is defined.

Reply: As the reviewer suggested, we addd a schematic diagram to describe the coordinate system used in this study.

5. line 106. I believe this references Eq. (8) not (7).
Reply: This is our mistake and we corrected it.

6. line 109. g_a is introduced without being defined as far as I can tell. This is referred to as aerodynamic conductance but some may be more familiar with it as a surface exchange coefficient for temperature. Is it simply the heat flux divided by the temperature difference? This should be explained.
Reply: The reviewer pointed out, we revised the texts with more information on the definitions of aerodynamic conductances.

7. Table 1 shows a z_0, but this is probably only in the control experiment as z_0 is calculated by the new scheme.
Reply: As the reviewer suggested, we revised the manuscript to clarify this issue.

8. With the iterations required, does this add much to the cost of the scheme in computer time.
Reply: Based on our simulation, the YSL scheme increased the computing time by only 8%. We believe that our scheme is promising because of improvement of meteorology simulation described in our manuscript accordingly. We added this information into the revised manuscript.

9. Figure 3. In the idealized case, the control z_0 is 0.25 m. Here the figure shows a ratio of z_0/z_{0N}. What is z_{0N} so that we can compare it with 0.25 m?
Reply: z0N is the value of z_0 in neutral conditions simulated by the new RSL model and thus Figure 3 shows the dependency of the roughness length with L_c/L by normalizing it with the roughness length in neutral condition. As the reviewer suggested, we revised the texts to clarify the definition of z_{0N}.

10. Figure 5 is another place where it would have helped to know that the original displacement height is less than the canopy height because we see the CTL values end there
Reply: As the reviewer pointed out, z/h must be $\tilde{z}/h$ in this figure. We revised the Figures. We appreciate your support for our manuscript and thank you.

Reply to reviewer 2

General comments:

Please check the language used in the paper (grammar and spelling; see also specific comments below). A key argument for the introduction of the roughness sublayer parameterization in WRF is the increase in computational power and the refinement of the vertical layers in the model. However, in the presentation of the simulations, no reference is made to how many vertical levels are used in the offline or real-case simulations. I encourage the authors to add this information. I would also encourage providing a note on how much more compute time is required in WRF, compared to the original MM5 approach.

Reply: As the reviewer suggested, we checked the language in our manuscript. We also revised our manuscript by providing the number of vertical layers and the computing time. In summary, the YSL scheme increased the computing time by only 8% compared to the original MM5 surface layer scheme. We believe that our scheme is promising because of improvement of meteorology simulation described in our manuscript accordingly.

Specific comments:

1. line 12 vs line 26: British or American English? line 12, modelling, is British English; line 26, parameterized, is American English. Please agree on one spelling and make the paper consistent.

Reply: We revised the manuscript with consistent English as the reviewer suggested.

2. line 20: for better weather and climate simulations (s in simulations missing)

Reply: We corrected it as the reviewer suggested.

3. line 54: gradient of "wind and scalar" and their corresponding fluxes in the RSL should that be "wind and scalar variables"?

Reply: We corrected it as the reviewer suggested.

4. line 65-66: "to implement it to the SL parameterization" "to implement it in the SL parameterization"?

Reply: We corrected it as the reviewer suggested.

5. line 68: "to incorporate RSL parameterization" "to incorporate the RSL parameterization"

Reply: We corrected it as the reviewer suggested.

6. lines 76-86: this section would benefit greatly from a schematic of the vertical layout (from surface to RSL-ISL interface).

Reply: As the reviewer suggested, we added a schematic diagram and revised our manuscript with a schematic diagram.

7. Section 2: all variables that are used need to be introduced, for example: l_m, β_N, f, ϕ_m.
Reply: Please consider that all variables are defined in Appendix A and we clarified this point in our revised manuscript.

8. lines 99-100: "because theoretical consistency" "because of theoretical consistency"
Reply: We corrected it as the reviewer suggested.

9. line 105: "iteratively update d_t and β using Eqs. (5) and (6)" "iteratively update d_t and β using Eqs. (5) and (7)"?
Reply: We corrected it as the reviewer suggested.

10. line 106: "z_0 is iteratively achieved with an accuracy of 0.0001 using Eq. (7)" "z_0 is iteratively achieved with an accuracy of 0.0001 using Eq. (8)"?
Reply: We corrected it as the reviewer suggested.

11. line 113-115: please rewrite this sentence and the short sentence in line 115.
Reply: We revised this sentence as the reviewer suggested.

12. section 4 - vertical layers used in the experiments?
Reply: We provided the information in section 3 and section 4, as the reviewer suggested.

13. section 6 - please check the language in particular in this section.
Reply: We received the English proof service for this section as the reviewer suggested.

14. line 200 - I would make the discussion of the summer season a new paragraph.
Reply: As the reviewer suggested, we made the discussion of the summer season a new paragraph.

15. line 205-206: check language of this sentence.
Reply: We received the English proof service for this section as the reviewer suggested.

16. line 228: "these changes in the climate near the ground surface" - is climate the correct term to use here? also, "ground surface" could be just "ground" or "surface"?
Reply: We revised the sentence as the reviewer suggested.

Reply to the editor

General comments:

This is an executive editor comment highlighting the ways in which this manuscript is not currently compliant with GMD policy on code and data availability. The following issues need to be resolved in any revised manuscript.

Reply: We revised the manuscript to comply with GMD policy on code and data availability. Please check our revision described below and let us know if you have further concern on GMD policy. Thank you very much.

Specific comments:

1. Github URLs. Github is an excellent development platform, but it lacks the features required of an archive. GitHub themselves tell authors to use Zenodo for this purpose. The authors should follow the procedure detailed there to archive the exact version of the software used to create the results presented: https://guides.github.com/activities/citable-code/. The resulting Zenodo repositories present the correct bibliography entries to use.

Reply: We made Zenodo repository of our codes (http://doi.org/10.5281/zenodo.3555537) as the editor suggested and showed this address in the revised manuscript.

2. Posting a URL is not a correct way to cite NCEP data. Click on the URL you posted and the very web site you go to provides information on how to cite, including buttons to download the appropriate BibTeX or RIS. Please cite this data properly

Reply: We revised the manuscript as the editor suggested.

3. The forcing data from the Korea Meteorological Administration is not identified with any precision at all. Please cite the specific data used so that someone who wished to reproduce your work would be able to find the exact data you used. It would also be particularly advantageous if the data could be found without having to read Korean, as I suspect that Korean literacy rates among the wider atmospheric science community are rather low.

Reply: We provided more details on the observation data in the revised manuscript with a full link address. Please consider the Korea Meteorological Administration provides data on website in Korean only and so in Code and data availability, we showed that the observation data were available upon request to the corresponding author (jhong@yonsei.ac.kr / http://eapl.yonsei.ac.kr).

Implementation of a roughness sublayer parameterization in the Weather Research and Forecasting model (WRF version 3.7.1) and its validation for regional climate simulations

Junhong Lee[1,2], Jinkyu Hong[1], Yign Noh[1], Pedro A. Jiménez[3]

[1]Department of Atmospheric Sciences, Yonsei University, Seoul, ~~South~~ Korea (Republic of)
[2]~~Max~~[2]current affiliation: Max Planck Institute for Meteorology, ~~Bundesstraße 53, 20146~~ Hamburg, Germany
[3]Research Application Laboratory, National Center for Atmospheric Research, Boulder, CO, USA

Correspondence to: Jinkyu Hong (jhong@yonsei.ac.kr)

Abstract. The roughness sublayer (RSL) is one compartment of the surface layer (SL) where turbulence deviates from Monin–Obukhov similarity theory. As the computing power increases, model grid sizes approach to the gray zone of turbulence in the energy containing range and the lowest model layer is located within the ~~RLS~~RSL. In this perspective, the RSL has an important implication in atmospheric ~~modelling~~modeling research. However, it has not been explicitly simulated in atmospheric mesoscale models. This study incorporates the RSL model proposed by Harman and Finnigan (2007, 2008) into the Jiménez et al. (2012) SL scheme. A high-resolution simulation performed with the Weather Research and Forecasting model (WRF) illustrates the impacts of the RSL parameterization on the wind, air temperature, and rainfall simulation in the atmospheric boundary layer. As the roughness parameters vary with the atmospheric stability and vegetative phenology in the RSL model, our RSL implementation reproduces the observed surface wind, particularly over tall canopies in the winter season by reducing the root mean square error (RMSE) from 3.1 to 1.8 m s^{-1}. Moreover, the improvement is relevant to air temperature (from 2.74 to 2.67 K of RMSE) and precipitation (from 140 to 135 mm $month^{-1}$ of RMSE~~), although its impact is not as substantial as that to wind speed.~~). Our findings suggest that the RSL must be properly considered both for better weather and climate ~~simulation~~simulations and for the application of wind energy and atmospheric dispersion.

1 Introduction

The Planetary boundary layer (PBL) is important for the proper simulation of weather, climate, wind energy application, and air pollution. Turbulence plays a critical role in the spatio–temporal variation of the PBL structure through the turbulent exchanges of momentum, energy, and water between the atmosphere and Earth's surface. Because turbulent eddies in the PBL are smaller than the typical grid size in mesoscale and global models, their impacts must be properly parameterized for atmospheric models. The surface layer (SL) occupies the lowest 10% of the ABL, where the shear-driven turbulence is dominant. In the SL, Monin–Obukhov similarity theory (MOST), which is a zero-order turbulence closure, provides the relationships between the vertical distribution of wind and scalars and the corresponding fluxes in a given stability condition

(Obukhov, 1946; Monin and Obukhov, 1954). The typical numerical weather prediction (NWP) and climate models are applied for the SL parameterization based on MOST to parameterize the subgrid-scale influences of the turbulent eddies in the PBL (e.g., Sellers et al., 1986, 1996).

The SL has two parts: inertial sublayer (ISL) and roughness sublayer (RSL). The ISL is the upper part of the SL, where MOST is valid and vertical variation of the turbulent fluxes is negligible. The RSL is the layer near and within the surface roughness elements (e.g., trees and buildings). The turbulent transport in the RSL has a mixing layer analogy, and the atmospheric flow depends on the roughness element properties (Raupach et al., 1996). Accordingly, the flux–gradient relationships in the RSL deviate from the MOST predictions, and the eddy diffusion coefficients are larger than the values in the ~~SL~~ISL (e.g., Shaw et al., 1988; Kaimal and Finnigan, 1994; Brunet and Irvine, 2000; Finnigan, 2000; Hong et al., 2002; Dupont and Patton, 2012; Shapkalijevski et al., 2016; Zhan et al., 2016; Basu and Lacser, 2017).

Traditionally, the RSL has not been explicitly considered in global and mesoscale models because the PBL in the model is coarsely resolved, and the lowest model layer is well above the roughness elements accordingly. As the computing power increases, the regional and global models can be simulated with a finer spatial resolution and the grid size of the NWP model moving toward the gray zone of turbulence (the scales on the order of the energy-containing range of turbulence). Nevertheless, studies on the impact of a fine vertical resolution have not been relatively performed. In this perspective, the RSL has an important implication in atmospheric ~~modelling~~modeling research. The lowest model layer is typically approximately 30 m high, and its vertical resolution continues to be better; hence, the models have more than one vertical layer in the RSL, which extends to 2–3 times of the canopy height. Furthermore, model outputs are sensitive to the selection of the lowest model level height (Shin et al., 2011), but its relation to the RSL has not yet been clearly investigated. Accordingly, turbulent transport in the RSL must be incorporated particularly in the mesoscale models if the vertical model levels are inside the RSL with an increase in the vertical model resolution.

The RSL function is a popular and simple method of incorporating the effects of the RSL in the observation and model (e.g., Raupach, 1992; Physick and Garratt, 1995; Wenzel et al., 1997; Mölder et al., 1999; Harman and Finnigan, 2007, 2008; de Ridder, 2010; Arnqvist and Bergström, 2015). The RSL function is defined as the observed relationship between the vertical gradient of wind and scalar variables and their corresponding fluxes in the RSL. Accordingly, simple relationships are appropriate for the land surface model in the climate model and for the mesoscale model (Physick and Garratt, 1995; Sellers et al., 1986, 1996). Despite the importance of the RSL, the Weather and Research Forecasting (WRF) model (Skamarock et al., 2008), which is one of the widely used models in the operation and research fields, does not consider the effects of the RSL~~, and has not yet been evaluated in~~ for the regional weather and climate simulations. Harman and Finnigan (2007, 2008) and Harman (2012) (hereafter, HFs) recently proposed a relatively simpler RSL function that can be used in a wide range of atmospheric models. The RSL function of the HFs is based on a theoretical background and applicable to a wide range of atmospheric stabilities by succinctly satisfying the continuity of the vertical profiles of fluxes, wind, and scalars both at the top of the RSL and at the top of a canopy. The parameterization of HFs has recently been incorporated in a one-dimensional (1D) PBL model and a land surface model (Harman, 2012; Shapkalijevski et al., 2017; Bonan et al., 2018).

Based on the abovementioned background, this study incorporates the RSL parameterization based on the RSL function of the HFs into the WRF model (version 3.7.1). For this purpose, we reformulate the HFs' RSL parameterization to implement it ~~to~~in the SL parameterization in the WRF model and then discuss the impacts of the RSL parameterization on the regional weather and climate simulations in terms of meteorological conditions near the Earth surface. To the best of the authors' knowledge, our study is the first extensive attempt to incorporate the RSL parameterization into the WRF model and to validate it for regional climate simulations. Section 2 is a brief discussion of the RSL parameterization of HFs and the implementation procedures into the WRF model. Section 3 explains the experimental and observational descriptions. Section 4 presents the impacts of the RSL parameterization. Section 5 ends the study with the concluding remarks.

2 RSL theory of the HFs

The roughness sublayer parameterization by HFs is adopted herein along with an explanation of the core of the HF model, and the relevant details on this parameterization can be found in Harman and Finnigan (2007, 2008) and Harman (2012). Appendix A lists ~~in alphabetical order~~ the symbols and variables used in this study in alphabetical order.

We first define the coordinate alignment for its application to the WRF. The revised MM5 SL scheme in the WRF model defines the vertical origin by the conventional zero-plane displacement height (d_0). The same coordinate system is also applied herein. The vertical coordinates z and $\tilde{z}$ in this coordinate system are defined as the distance from d_0 and from the terrain surface, respectively; therefore, their relation is $z = \tilde{z} - d_0$. (Fig. 1). Note that a vertical origin in the HFs is at the canopy height (h). MOST says that a variable (C), such as wind speed (u) and temperature (T), has the logarithmic vertical profile:

$$\frac{k}{C_*}(C(z) - C_0) = \ln\left(\frac{z}{z_0}\right) - \psi_c\left(\frac{z}{L}\right) + \psi_c\left(\frac{z_0}{L}\right), \quad (1)$$

where k is von Kármán constant; C_* is a C scale; C_0 is C at z_0; z_0 is the roughness length; ψ_c is the integrated similarity function of C; and L is the Obukhov length. The C profile based on the RSL function of the HFs is divided into two layers depending on the relative distance between ~~h~~the canopy height (h) and the redefined zero-plane displacement height in the HFs ($d_t = h - d_0$): the upper-canopy layer ($z > d_t$), where the influence of additional mixing by the canopy exists, and the lower-canopy layer ($z < d_t$), where the canopy is the direct source and sink for drag and heat. The vertical profile in the upper-canopy layer is described as follows:

$$\frac{k}{C_*}(C(z) - C_0) = \ln\left(\frac{z}{z_0}\right) - \psi_c\left(\frac{z}{L}\right) + \psi_c\left(\frac{z_0}{L}\right) + \int_z^\infty \frac{\phi_c(1-\hat{\phi}_c)}{z'}dz', \quad (2)$$

where ϕ_c is the similarity function of C and $\hat{\phi}_c$ is an RSL function of C. In the $z \to \infty$ limit, $\hat{\phi}_c$ is equal to 1 and the wind speed converges to the MOST prediction. The last term in the right-hand side represents the additional mixing caused by the roughness element due to the coherent canopy turbulence, and can be replaced by $\hat{\psi}_c$, which is an integrated RSL function of C. The vertical profile from the HFs for the RSL deviates from that of MOST because of $\hat{\psi}_c$, thereby adjusting the logarithmic profile. The $\hat{\phi}_c$ is introduced as follows:

$$\hat{\phi}_c = 1 - c_1 \exp\left[-c_2 \frac{\beta}{l_m} z\right]. \quad (3)$$

~~The~~c_1 and c_2 are then determined from the continuity of $\hat{\phi}_c$ at the canopy top and the RSL function, $\hat{\phi}_c$ exponentially converges to zero above the RSL. ~~c_1 and c_2 are then determined from the continuity of $\hat{\phi}_c$ at the canopy top.~~ In the lower canopy layer, C has the following exponential form:

$$C(z) - C_0 = (C_h - C_0) \exp\left(f \frac{z - d_t}{2d_t}\right), \quad (4)$$

The RSL functions vary with atmospheric stability through β,

$$\beta = \begin{cases} \frac{\beta_N}{\phi_m(z=d_t)} & \frac{L_c}{L} > -0.15 \\ \frac{k}{2\phi_m(z=d_t)} + \frac{\frac{\beta_N}{\phi_m(z=d_t)} - \frac{k}{2\phi_m(z=d_t)}}{1+2\left|\frac{L_c}{L}+0.15\right|^{1.5}} & \frac{L_c}{L} \leq -0.15 \end{cases}, \quad (5)$$

where L_c is a canopy penetration depth defined as:

$$L_c = (c_d a)^{-1} = \frac{4h}{LAI}. \quad (6)$$

where c_d is a drag coefficient at the leaf scale and a is the leaf area density. The parameter d_t and z_0 also depend on the stability because of their dependence on β:

$$d_t = h - d_0 = \frac{l_m}{2\beta} = \beta^2 L_c, \quad (7)$$

$$z_0 = d_t \exp\left[-\frac{k}{\beta}\right] \exp\left[-\psi_m\left(\frac{d_t}{L}\right) + \psi_m\left(\frac{z_0}{L}\right)\right] \exp\left[\int_{d_t}^{\infty} \frac{\phi_m(1-\hat{\phi}_m)}{z'} dz'\right]. \quad (8)$$

~~where ψ_m is the integrated similarity function for the momentum.~~

3 Incorporation of the roughness sublayer parameterization into the WRF model

The RSL parameterization of the HFs described above is implemented in the Jiménez et al. (2012) revised MM5 surface layer scheme and Noah land surface model in the WRF (hereafter called the Yonsei University surface layer (YSL) scheme) because of theoretical consistency between the HFs and PBL parameterization. To incorporate the RSL parameterization, it is necessary to modify the SL scheme and the land surface model as follow (Fig. 1): the first step is to compute the bulk Richardson number at the lowest model layer, Bi_b, by the original equation of Jiménez et al. (2012) [Eq. (9) in their study]:

$$Bi_b = \frac{g}{\theta_a} \frac{\theta_{va} - \theta_{vg}}{[U(z_r)]^2} \frac{\theta_{va} - \theta_{vg}}{[u(z_r)]^2} z_r. \quad (9)$$

The second step is to iteratively calculate the atmospheric stability (z_r/L) as follows with an accuracy of 0.01:

$$\frac{z_r}{L} = Bi_b \frac{\left[\ln\left(\frac{z_r}{z_0}\right) - \psi_m\left(\frac{z_r}{L}\right) + \psi_m\left(\frac{z_0}{L}\right) + \hat{\psi}_m\right]^2}{\left[\ln\left(\frac{\rho c_p k u_*^{n-1} z_r}{c_s} + \frac{z_r}{z_l}\right) - \psi_h\left(\frac{z_r}{L}\right) + \psi_h\left(\frac{z_l}{L}\right) + \hat{\psi}_h\right]}, \quad (10)$$

where u_*^{n-1} is the friction velocity (u_*) at previous time step. Equation (10) is different from Eq. (23) of Jiménez et al. (2012) by the RSL functions (i.e., $\hat{\psi}_m$ and $\hat{\psi}_h$). After z_r/L is determined, the third step is to iteratively update d_t and β using Eqs. (5) and (~~6~~7) with an accuracy of 0.0001 because they are inter-correlated with each other. Subsequently, z_0 is iteratively achieved with an accuracy of 0.0001 using Eq. (~~7~~8) at the given z_r/L, β, and d_t. The u profile is determined using Eqs. (2) and (4). Following Jiménez et al. (2012), the profile of a scalar, such as T, is determined by

$$\frac{k}{C_*}(C(z) - C_0) = \ln\left(\frac{\rho c_p k u_*^{n-1} z_r}{c_s} + \frac{z_r}{z_l}\right) - \psi_c\left(\frac{z}{L}\right) + \psi_c\left(\frac{z_0}{L}\right) + \int_z^\infty \frac{\phi_c(1-\tilde{\phi}_c)}{z'} dz', \quad (11)$$

for the upper-canopy layer. Equation (4) is used for the lower-canopy layer. Finally, u_* ~~and the aerodynamic conductance (g_a) in the RSL are~~is given to

$$u_* = \frac{ku(z_r)}{\left[\ln\left(\frac{z_r}{z_0}\right) - \psi_m\left(\frac{z_r}{L}\right) + \psi_m\left(\frac{z_0}{L}\right) + \hat{\psi}_m\right]} \quad (12)$$

~~and,~~

~~$g_{a1} = \frac{\ln\left(\frac{z_r}{d_t}\right) - \psi_h\left(\frac{z_r}{L}\right) + \psi_h\left(\frac{d_t}{L}\right) + \hat{\psi}_h\left(\beta\frac{z_r}{l_m}\right) - \hat{\psi}_h\left(\beta\frac{d_t}{l_m}\right)}{ku_*}$,~~

~~$g_{a2} = \frac{S_c}{\beta^2 u_h}\left[\exp\left(\beta\frac{d_t - z_l}{l_m}\right) - 1\right]^{-1}$,~~

~~$g_{a3} = \frac{\ln\left(\frac{\rho c_p k u_*^{n-1} z_l}{c_s} + 1\right)}{ku_*}$ and~~

~~$g_a = \frac{1}{1/g_{a1} + 1/g_{a2} + 1/g_{a3}}$.~~and the aerodynamic conductance from z=0 to $z = z_r$ (g_a) in the RSL are given to

$$1/g_a = \int_0^{z_r} \frac{dz}{K_h(z)} \equiv 1/g_{a1} + 1/g_{a2} + 1/g_{a3} \quad (13)$$

$$1/g_{a1} \equiv \int_0^{z_l} \frac{dz}{K_h(z)} = \int_0^{z_l} \frac{dz}{ku_* z + \frac{c_s}{\rho c_p}} = \frac{1}{ku_*} \ln\left[\frac{ku_* z_l}{c_s/\rho c_p} + 1\right]$$

$$1/g_{a2} = \int_{z_l}^{d_t} \frac{dz}{K_h(z)} = \frac{S_c}{\beta^2 u_h}\left[\exp\left(\beta\frac{d_t - z_l}{l_m}\right) - 1\right],$$

$$1/g_{a3} = \int_{d_t}^{z_r} \frac{dz}{K_h(z)} = \int_{d_t}^{z_r} \frac{\Phi_h}{ku_* z} dz = \frac{1}{ku_*}\left[\ln\left(\frac{z_r}{d_t}\right) - \psi_h\left(\frac{z_r}{L}\right) + \psi_h\left(\frac{d_t}{L}\right) + \hat{\psi}_h(\beta\frac{z_r}{l_m}) - \hat{\psi}_h\left(\beta\frac{d_t}{l_m}\right)\right].$$

Computing time increased only 8 % with 61 vertical layers in the YSL scheme despite more iterations in the YSL scheme compared to the revised MM5 SL scheme.

4 Numerical experimental design

This study evaluated the YSL scheme by making a 1D offline ~~test~~ and ~~a~~ real case ~~simulation~~simulations. The 1D offline ~~simulation was~~simulations were done to test the YSL scheme performance without feedback ~~to~~with the atmosphere. The ~~two~~ 1D offline ~~simulations are carried out; simulation~~ consisted of the YSL, and the revised MM5 SL schemes coupled with the Noah land surface model~~, and the Yonsei University (YSU) PBL scheme (hereafter~~ (i.e., offCTL and offRSL experiments~~).)~~ (Table 1 ~~presents~~). In the offline simulations, offCTL and offRSL indicate numerical experiments with and without the RSL parameterization, respectively and were driven by the idealized forcing data ~~for boundary condition,~~described in Table 1. The real case simulation consisted of two experiments: ~~one~~ reproducing 1 month ~~simulation during~~of winter (January 2016) with the ~~original~~ revised MM5 SL scheme and the YSL scheme (hereafter referred to as the rCTL and rRSL experiments). The rCTL and the rRSL employed the same physics package, except for the SL scheme and the land surface model (Lee and Hong, 2016 and references therein). One-way nesting was applied herein in a single-nested domain with a Lambert conformal map projection to East Asia (~~Fig. 2~~Figure 3). A 9 km horizontal resolution domain 2 was then embedded in the 27 km resolution domain 1 with ~~31~~61 vertical layers. The initial and boundary conditions were produced using the National Center for Environmental Prediction Final Analysis data (1° ~~×~~× 1°).

5 Observation data for the model validation

The model performance was examined against the surface wind speed ~~and the~~, surface temperature and precipitation observed at 46 Automated Synoptic Observing System (ASOS) sites in Korea (Fig. 2). Quality control of the data includes gap detection, limit test, step test based on the standard of the World Meteorological Administration and Korea Meteorological Administration (KMA) (Zahumensky, 2007; Hong et al., 2013). For the model validation of the real case simulation, the three different measures of the correlation coefficients, centered root–mean–square differences (RSMD), and standard deviations of the model (σ_m) normalized by that of the observation (σ_o) are together shown in a Taylor diagram (Taylor, 2001). In the Taylor diagram, a point nearer the observation at a reference point (OBS) can be considered to give a better agreement with the observation. We also provide the root–mean–square error (RMSE) and the mean bias (MB) with the pattern correlation for the rainfall simulation validation.

Formatted: English (United States)

6 Results

6.1 Offline simulations

Figure ~~3~~4 shows the roughness parameters (i.e., z_0, d_t, and β) as a function of the normalized atmospheric stability (L_c/L) from the 1D offline simulation of the YSL scheme~~. (offRSL).~~ The offline YSL simulations reproduced the results of ~~Harman and Finnigan (2007, 2008).~~HFs. The roughness parameters varied with the atmospheric stability, L_c/L, and had peaks at weakly unstable conditions. ~~Note that~~These dependencies of the roughness parameters on the atmospheric stability are distinct from typical manner of dealing with the roughness parameters as a constant in atmospheric models. The roughness length is indeed constant based on the land cover in ~~the traditional atmospheric model such as~~ all the SL schemes in the WRF.

Figure ~~4~~5 indicates that the impacts of the ~~roughness sublayer~~RSL are also ~~decided by~~function of L_c, which is a function of LAI and h (Eq. (6)), thus leading to both diurnal and seasonal variation of canopy roughness. Consequently, the roughness parameters showed daily and seasonal variations. Overall, the roughness length in the YSL was larger than the revised MM5 SL scheme, particularly in a smaller z/L (i.e., neutral and unstable conditions) and a larger L_c (i.e., small LAI and/or large h). The roughness length in a stable condition showed relatively smaller changes with z/L and L_c compared to those in the unstable condition. Our findings suggest that ~~L_c becomes larger~~ a small LAI in the winter season ~~over tall forest canopies~~ makes a larger L_c because of the smaller LAI~~, and higher h~~, thereby leading to relatively larger differences of z_0 between the YSL scheme and the default WRF scheme. On the contrary, a similar value of z_0 was observed in summer because of the larger LAI. Note that the revised MM5 SL scheme does not consider d_t and β.

The RSL function, $\hat{\phi}_c$, was introduced ~~by HFs, considers~~to consider the additional mixing caused by the roughness element. Accordingly, $\hat{\phi}_c$ should asymptotically converge to the MOST profile (i.e., $\hat{\phi}_c \rightarrow 1$) as z increases with the continuous vertical profiles of the wind and the temperature. The YSL scheme reproduced these properties of $\hat{\phi}_c$ and matched with the observed profiles inside canopies: the YSL scheme showed exponential profiles under the canopy top and logarithmic profiles above the canopy top (Fig. ~~5~~6). The wind speed and the air temperature above the canopy top were smaller than predicted by MOST because $\hat{\phi}_c < 1$ in the offRSL experiments. ~~Notably~~Furthermore, the YSL scheme produced wind and temperature ~~below~~within the ~~zero-plane displacement height,~~canopy (i.e. $\tilde{z} < z_0 + d_0$), thereby providing additional useful information on the atmospheric dispersion inside the canopy.

The roughness length changes in the YSL scheme eventually produced changes in the surface energy balance with the atmospheric stability (Fig. ~~6~~7). In the 1D offline simulations based on the conditions in Table 1, the YSL scheme produced a larger z_0 in the unstable and near-neutral conditions, but a smaller z_0 in $z/L > 3$ compared to the offCTL. The aerodynamic conductance (g_a) in the YSL scheme was larger in all the stability conditions even in the stable conditions in which the YSL provided a smaller z_0 because the additional term in Eq. (13), g_{a2}, dominated over the other effects in the g_a calculation. Accordingly, H and λE in the YSL scheme were larger than those in the revised MM5 SL scheme. Our finding implies stronger fluxes from the YSL scheme when the gradient of quantity is the same. However, the impact of the increased g_a was asymmetrical in H and λE depending on the soil moisture content. In this case simulation, an increase in λE was dominant

Formatted: English (United States)
Formatted: English (United States)
Formatted: English (United States)
Formatted: English (United States)
Formatted: English (United States)

because the wet condition made more partitioning of the available energy into the latent heat flux first in the model. However, in the dry condition (i.e., less soil water content), the YSL produced a larger H without a substantial increase of λE (Fig. S1). A significant increase in λE was found along with a decrease in H in the strong unstable conditions (Fig. ~~6~~7) because of the wet soil moisture of 0.25 m^3 m^{-3} in the offRSL simulation in Table 1. The slight increase in the net radiation was mainly associated with the reduced outgoing longwave radiation caused by the smaller surface temperature in the offRSL.

6.2 Real case simulations

Figure ~~7~~8 shows the real case simulation of the roughness length, 10 m wind speed (u_{10}), and 2 m air temperature (T_2). We discuss herein the real cases in the winter season because of stronger effect of the roughness sublayer. The results for the summer season can be found in the Supplementary Materials. The roughness length in the rCTL experiment was prescribed from the vegetation data table (i.e., VEGPARM table in the WRF model) and modified by the vegetation fraction (~~Figs. 2 and 7a~~Fig. 8a).

Overall, the YSL scheme (rRSL experiment) produced 0.2–2.0 m larger z_0 than the default values in the rCTL experiment over the tall canopies, where L_c was large. In contrast, the YSL scheme produced a similar or even slightly smaller z_0 over the short canopies compared to the rCTL experiment. Importantly, the changes of z_0 made direct impacts on the momentum fluxes and thus surface wind speed (Fig. ~~7b~~8b). The typical u_{10} in the rCTL was larger than approximately 3 m s^{-1}, and a much stronger wind (> 6 m s^{-1}) was observed along the mountains, making a positive bias against the observation. Overall, the YSL scheme reproduced the better observed diurnal variation by reducing the positive bias of the wind speed (Table 2, Fig. ~~8~~9). Over the tall forest canopies, u_{10} in the rRSL was reduced by approximately 30%; however, the region of the ~~smaller~~increased wind speed corresponded to the short canopies, where the roughness length increased (Figs. ~~7a~~8a and ~~b~~8b). The YSL scheme particularly provided better RMSD and correlation coefficient, but less diurnal variability of wind speed because of a relatively larger reduction of the daytime wind speed (Fig. ~~8~~9). MB and RMSE decreased from 2.4 m s^{-1} to 1.0 m s^{-1} and from 3.1 m s^{-1} and 1.8 m s^{-1}. The Taylor diagram shows that the overall performance of the YSL scheme is better than the default WRF simulation at all the 46 sites. In the Taylor diagram, the statistics moved toward the observation, except for one site, indicating an overall improvement of 2 m air temperature in the YSL scheme; however, the impact of the RSL was not as large as the wind speed (Table 2, Fig. ~~9~~10).

Similar to the increases of the aerodynamic conductance in the offline simulations, the YSL scheme in the real case simulation (i.e., the rRSL simulation) simulated a larger g_a, particularly in the forest canopies and mountain regions (Fig. ~~10a~~11a). This larger g_a in the YSL scheme led to the increases of the latent heat fluxes by approximately 20 W m^{-2}, with an eventual reduction of the soil water content (Fig. ~~11a~~12a). The sensible heat fluxes in the rCTL experiments were generally approximately 80 W m^{-2}, except over the snow-covered region where H was approximately 40 W m^{-2}. As described in the offline simulation, the changing sign of H in the rRSL depended on the soil moisture content because evapotranspiration is limited in dry soils at given available energy (Figs. ~~10b~~11b and ~~11b~~12b). Consequently, the available energy (=H + λE)

increased in the YSL scheme, and a larger λE in the rRSL led to a cooler temperature ~~cooler~~ than that in the rCTL experiment (Fig. ~~7c~~8c).

During the winter simulation period, precipitation was observed over an extensive area in the domain, and snow was dominant over the northeastern side of the domain (Figs. ~~11a~~12b and ~~12~~13). The overall total precipitation in the YSL scheme increased, and the skill score indicated a better simulation of the total amount of precipitation (Table 2, Fig. ~~12~~13). The pattern correlation of precipitation also increased from 0.972 to 0.978 in the YSL scheme based on 656 rain gauge stations, indicating a better match of the precipitation bands. Despite the increase in λE, precipitation decreased in several regions (Figs. ~~10b~~11b and ~~12b~~13b). The differences were not significant in the summer season, and the skill scores in the YSL scheme were similar to the default WRF simulation because our implemented RSL parameterization started to converge to the default WRF in a smaller L_c (i.e., ~~smaller~~larger *LAI* and/or ~~higher~~smaller h) and strong synoptic influences by the summer heavy rainy period (Table S1, Figs. S2–S6).

Formatted: English (United States)

7 Summary and conclusion remark

Turbulent fluxes regulate the planetary boundary layer; thus, they are a crucial process for weather, climate, and air pollution simulations. Most of the NWP and climate models are commonly applied for MOST to compute the turbulent fluxes near the Earth's surface. MOST can be~~, however,~~ only applicable in the inertial ~~sublayers~~layer, and turbulence deviates from MOST in the roughness sublayer. Importantly, roughness sublayer, the important compartment of the SL, has not been properly parameterized in the model. Increasing the computing power enables us to use more vertical layers in the atmospheric models. Accordingly, the RSL must be incorporated into the model properly to simulate the atmospheric processes in the gray zone. This study proposed the YSL scheme, which incorporated the RSL into the WRF model, based on the RSL model proposed by Harman and Finnigan (2007, 2008) and Harman (2012). We also investigated the impacts of the RSL parameterization on the weather and climate simulations. For these purposes, we designed a series of offline simulations with an idealized boundary condition and a real case simulation to evaluate the performance of the YSL scheme against the observation data.

Formatted: English (United States)

Formatted: English (United States)

Formatted: English (United States)

Formatted: English (United States)

Formatted: English (United States)

The 1D offline simulation revealed that the YSL scheme successfully reproduced the features ~~observed~~reported in various canopies ~~and Harman and Finnigan (2007, 2008).~~ The RSL function, $\hat{\phi}_c$, asymptotically increased to 1, and the vertical gradients of the wind speed and the temperature decreased in the RSL as z increased, thereby ~~deviating from~~converging to the MOST prediction. Notably, unlike the typical assignment of the roughness ~~parameter~~parameters (i.e., z_0, d_c, and β) as a constant, the roughness parameters ~~(i.e., z_0, d_c, and β)~~ are functions of the atmospheric stability (z/L) and L_c. The roughness parameters had a maximum in the weakly unstable condition and in larger L_c (i.e., large h or small *LAI*). In most conditions, the YSL scheme provided a larger roughness length, thereby producing a wind speed slower than that of the revised MM5 SL scheme. The YSL scheme simulated a colder surface temperature in the unstable conditions.

Meanwhile, the real case simulation showed that the RSL-incorporated WRF produced a larger z_0 than the default WRF. This increase in z_0 and its change with atmospheric stability eventually made substantial impacts on ~~the surface energy balance,~~

wind, and temperature near the ~~ground~~ surface, momentum transfer, surface energy balance, and precipitation. First, an increase of z_0 produced larger momentum fluxes and a smaller 10 m wind speed when the YSL scheme was applied, leading to the mitigation of ~~substantial~~ positive bias in the wind speed in the revised MM5 SL scheme. The larger z_0 also made increases in the available energy. This increased available energy is related to the surface cooling caused by the increases in the latent heat fluxes in the wet surface conditions when the RSL parameterization is applied. As a result, these changes in the climate near the ~~ground~~ surface and the surface energy balance ~~regulated~~resulted in more precipitation, thereby giving a better simulation of the amount of precipitation and its spatial pattern.

Our results indicate that the RSL parameterization can be a promising option for resolving the typical overestimation of the surface wind speed of the WRF model, particularly in the tall vegetation and low LAI, ~~despite a relatively larger~~with slight increase of computing time (e.g., Hu et al., 2010, 2013; Shimada and Ohsawa, 2011; Shimada et al., 2012; Wyszogrodzki et al., 2013; Lee and Hong, 2016). The improvement caused by the RSL parameterization is useful in air quality ~~modelling~~modeling and wind energy estimation by better weather and climate in the planetary boundary layer. A further study is necessary to evaluate the characteristics of the YSL scheme in various cases particularly at gray-zone resolutions.

Code and data availability. The source code of the Weather Research and Forecasting Model (WRF) is available at http://www2.mmm.ucar.edu/wrf/users/downloads.html. The source code of the YSL scheme and the ~~modelling~~modeling output presented in this study are available at ~~Github (https://github.com/Yonsei-EAPL/JunhongLee/blob/master/module_sf_ysl.F~~Zenodo (http://doi.org/10.5281/zenodo.3555537). The National Center for Environmental Prediction Final Analysis data that was used as initial and boundary conditions is available at https://rda.ucar.edu/datasets/ds083.2~~/. The observed wind speed, temperature, and precipitation~~ (National Centers for Environmental Prediction, National Weather Service, NOAA, U.S. Department of Commerce, 2000). The observation data used for the model validation can be downloaded at the Korea Meteorological Administration data portal (https://data.kma.go.kr/~~emmn/main.do~~data/grnd/selectAsosRltmList.do?pgmNo=36) or are available upon request to the corresponding author (jhong@yonsei.ac.kr / http://eapl.yonsei.ac.kr).

Formatted: Font: Bold, Font color: Black, Kern at 16 pt

Appendix A: List of symbols and definitions

Symbols	Definitions
$\boldsymbol{a}$	Leaf are density
$\boldsymbol{Bi_b}$	Bulk Richardson number, at the lowest model layer
$\boldsymbol{c_d}$	Drag coefficient at the leaf level
$\boldsymbol{c_p}$	Specific heat for air
$\boldsymbol{c_s}$	Effective heat transfer coefficient for nonturbulent processes (Carlson and Boland, 1978; Jiménez et al., 2012)
$\boldsymbol{C}$	Variable at z, such as u and T
$\boldsymbol{C_0}$	C at $z = z_0$
$\boldsymbol{C_h}$	C at h
$\boldsymbol{C_*}$	Scale of C
$\boldsymbol{d_0}$	Conventionally defined zero-plane displacement height
$\boldsymbol{d_t}$	Redefined zero-plane displacement height in Harman and Finnigan (2007)
$\boldsymbol{f}$	Parameter related the depth scale of the scalar profile ($\equiv \frac{1}{2}(\sqrt{1 + 4r_c S_r} - 1)$)
$\boldsymbol{g}$	Gravitational acceleration
$\boldsymbol{g_a}$	Aerodynamic conductance
$\boldsymbol{h}$	Canopy height
$\boldsymbol{k}$	von Kármán constant
$\boldsymbol{l_m}$	Mixing length for momentum
$\boldsymbol{L}$	Obukhov length
$\boldsymbol{L_c}$	Canopy penetration depth ($\equiv (c_d a)^{-1} = \frac{4h}{LAI}$)
$\boldsymbol{LAI}$	Leaf area index

$\boldsymbol{p}$	Pressure at z
$\boldsymbol{q}$	Water vapor mixing ratio at z
$\boldsymbol{r_c}$	Canopy Stanton number
$\boldsymbol{SW}$	Downward shortwave radiation
$\boldsymbol{S_c}$	Turbulent Schmidt number
$\boldsymbol{S_m}$	Soil ~~mositure~~moisture
$\boldsymbol{S_r}$	Turbulent Schmidt number
$\boldsymbol{T}$	Air temperature at z
$\boldsymbol{T_2}$	Air temperature at 2 m
$\boldsymbol{T_{sk}}$	Skin temperature
$\boldsymbol{u}$	Wind speed at z
$\boldsymbol{u_{10}}$	Wind speed at 10 m
$\boldsymbol{u_h}$	Wind speed at h
$\boldsymbol{u_*}$	Friction velocity
$\boldsymbol{u_*^{n-1}}$	Previous time step value of u_*
$\boldsymbol{z}$	Height from d_0
$\boldsymbol{\tilde{z}}$	Height from terrain surface
$\boldsymbol{z_0}$	Roughness length
$\boldsymbol{z_l}$	Viscous sublayer depth =0.001 (Carlson and Boland, 1978; Jiménez et al., 2012)
$\boldsymbol{z_r}$	Hight of the lowest model layer
$\boldsymbol{z_r/L}$	Atmospheric stability
$\boldsymbol{\beta}$	u_*/u_h

$\boldsymbol{\beta_N}$	β at neutral condition (=0.374)
$\boldsymbol{\theta_a}$	Potential temperature of the air at z_r
$\boldsymbol{\theta_{va}}$	Virtual potential temperature of the air at z_r
$\boldsymbol{\theta_{vg}}$	Virtual potential temperature of the air at ground
$\boldsymbol{\rho}$	Density of air
$\boldsymbol{\phi_C}$	Similarity function of C
$\boldsymbol{\widehat{\phi}_C}$	RSL function of C
$\boldsymbol{\psi_C}$	Integrated similarity function of C
$\boldsymbol{\psi_h}$	Integrated similarity function of heat
$\boldsymbol{\psi_m}$	Integrated similarity function of momentum
$\boldsymbol{\widehat{\psi}_C}$	Integrated RSL function of C
$\boldsymbol{\widehat{\psi}_h}$	Integrated RSL function of heat
$\boldsymbol{\widehat{\psi}_m}$	Integrated RSL function of momentum

Author contribution. JL and JH contributed to the code development for the YSL scheme, data analysis, and manuscript preparation. YN and PAJ contributed to the writing and editing of the paper and data analysis.

Competing interests. The authors declare that they have no conflict of interest.

Acknowledgements. This publication was supported by the National Research Foundation of Korea grant funded by the Korean government (MSIT) (NRF-2018R1A5A1024958), the Korea Meteorological Administration Research and Development Program under Grant KMI2018-03512, and the Korea Polar Research Institute (KOPRI, ~~PN19081~~PN20081).

References

Arnqvist, J. and Bergström, H.: Flux-profile relation with roughness sublayer correction, Q. J. Roy. Meteor. Soc., 141, 1191-1197, 2015.

Barlow, J. and Coceal, O.: A review of urban roughness sublayer turbulence, Tech. Rep., No. 527, 68 pp., 2008.

Basu, S. and Lacser, A.: A Cautionary Note on the Use of Monin–Obukhov Similarity Theory in Very High-Resolution Large-Eddy Simulations, Bound.-Lay. Meteorol., 163, 351-355, 2017.

Bonan, G. B., Patton, E. G., Harman, I. N., Oleson, K. W., Finnigan, J. J., Lu, Y., and Burakowski, E. A.: Modeling canopy-induced turbulence in the Earth system: a unified parameterization for turbulent exchange within plant canopies and the roughness sublayer (CLM-ml v0), Geosci. Model Dev., 11, 1467-1496, 2018.

Brunet, Y. and Irvine, M. R.: The control of coherent eddies in vegetation canopies: streamwise structure spacing, canopy shear scale and atmospheric stability, Bound.-Lay. Meteorol., 94, 139-163, 2000.

Carlson, T. N. and Boland, F. E.: Analysis of urban-rural canopy using a surface heat flux/temperature model, Bound.-Lay. Meteorol., 17, 998-1013, 1978.

de Ridder, K.: Bulk transfer relations for the roughness sublayer, Bound.-Lay. Meteorol., 134, 257-267, 2010.

Dupont, S. and Patton, E. G.: Momentum and scalar transport within a vegetation canopy following atmospheric stability and seasonal canopy changes: the CHATS experiment, Atmos. Chem. Phys., 12, 5913-5935, 2012.

Finnigan, J. J.: Turbulence in plant canopies, Annu. Rev. Fluid Mech., 32, 519-571, 2000.

Harman, I. N.: The role of roughness sublayer dynamics within surface exchange schemes, Bound.-Lay. Meteorol., 142, 1-20, 2012.

Harman, I. N. and Finnigan, J. J.: A simple unified theory for flow in the canopy and roughness sublayer, Bound.-Lay. Meteorol., 123, 339-363, 2007.

Harman, I. N. and Finnigan, J. J.: Scalar concentration profiles in the canopy and roughness sublayer, Bound.-Lay. Meteorol., 129, 323-351, 2008.

Hong, J., Kim, J., Miyata, A., and Harazono, Y.: Basic characteristics of canopy turbulence in a homogeneous rice paddy, J. Geophys. Res., 107, ACH-8, 2002.

Hong, J.-W., Hong, J., Lee, S., and Lee, J.: Spatial distribution of urban heat island based on local climate zone of automated weather station in Seoul metropolitan area, 23, 1-12, 2013 (In Korean with English abstract)

Hu, X. M., Nielsen-Gammon, J. W., and Zhang, F.: Evaluation of three planetary boundary layer schemes in the WRF model, J. Appl. Meteorol. Clim., 49, 1831-1844, 2010.

Hu, X. M., Klein, P. M., and Xue, M.: Evaluation of the updated YSU planetary boundary layer scheme within WRF for wind resource and air quality assessments, J. Geophys. Res., 118, 10-490, 2013.

Jiménez, P. A., Dudhia, J., González-Rouco, J. F., Navarro, J., Montávez, J. P., and García-Bustamante, E.: A revised scheme for the WRF surface layer formulation, Mon. Weather Rev., 140, 898-918, 2012.

Kaimal, J. C., and Finnigan, J. J.: Atmospheric boundary layer flows: their structure and measurement, Oxford University Press, United Kingdom, 1994.

Lee, J. and Hong, J.: Implementation of spaceborne lidar-retrieved canopy height in the WRF model, J. Geophys. Res., 121, 6863–6876, 2016.

Mölder, M., Grelle, A., Lindroth, A., and Halldin, S.: Flux-profile relationships over a boreal forest—roughness sublayer corrections, Agr. Forest Meteorol., 98, 645-658, 1999.

Monin, A. S. and Obukhov, A. M. F.: Basic laws of turbulent mixing in the surface layer of the atmosphere, Contributions of the Geophysical of the Slovak Academy of Sciences, 151, 163-187, 1954.

Obukhov, A. M.: Turbulence in an atmosphere with a nonuniform temperature, Trudy Inst. Theor. Geofiz. AN SSSR, 1, 95–115, 1946.

Physick, W. L. and Garratt, J. R.: Incorporation of a high-roughness lower boundary into a mesoscale model for studies of dry deposition over complex terrain, Bound.-Lay. Meteorol., 74, 55-71, 1995.

Raupach, M.: Drag and drag partition on rough surfaces, Bound.-Lay. Meteorol., 60, 375-395, 1992.

Raupach, M., Finnigan, J. J., and Brunet, Y.: Coherent eddies and turbulence in vegetation canopies: the mixing-layer analogy, Springer, Netherlands, 1996.

Sellers, P. J., Mintz, Y. C. S. Y., Sud, Y. E. A., and Dalcher, A.: A simple biosphere model (SiB) for use within general circulation models, J. Atmos. Sci., 43, 505-531, 1986.

Sellers, P. J., Randall, D. A., Collatz, G. J., Berry, J. A., Field, C. B., Dazlich, D. A., Zhang, C., Collelo, G. D., and Bounoua, L.: A revised land surface parameterization (SiB2) for atmospheric GCMs. Part I: Model formulation, J. Climate, 9, 676-705, 1996.

Shapkalijevski, M. M., Moene, A. F., Ouwersloot, H. G., Patton, E. G., and Vilà-Guerau de Arellano, J.: Influence of Canopy Seasonal Changes on Turbulence Parameterization within the Roughness Sublayer over an Orchard Canopy, J. Appl. Meteorol. Clim., 55, 1391-1407, 2016.

Shapkalijevski, M. M., Ouwersloot, H. G., Moene, A. F., and Arrellano, J. V. G. D.: Integrating canopy and large-scale effects in the convective boundary-layer dynamics during the CHATS experiment, Atmos. Chem. Phys., 17, 1623-1640, 2017.

Shaw, R. H., Den Hartog, G., and Neumann, H. H.: Influence of foliar density and thermal stability on profiles of Reynolds stress and turbulence intensity in a deciduous forest, Bound.-Lay. Meteorol., 45, 391-409, 1988.

Shimada, S. and Ohsawa, T.: Accuracy and characteristics of offshore wind speeds simulated by WRF, Sola, 7, 21-24, 2011.

Shimada, S., Ohsawa, T., Chikaoka, S., and Kozai, K.: Accuracy of the wind speed profile in the lower PBL as simulated by the WRF model, Sola, 7, 109-112, 2011.

Shin, H. H., Hong, S. Y., and Dudhia, J.: Impacts of the lowest model level height on the performance of planetary boundary layer parameterizations, Mon. Weather Rev., 140, 664-682, 2012.

Skamarock, W. C. and Coauthors: A description of the Advanced Research WRF version 3, Tech. Rep., Note NCAR/TN-4751STR, 113 pp., doi: 10.5065/D68S4MVH, 2008.

Taylor, K. E.: Summarizing multiple aspects of model performance in a single diagram, J. Geophys. Res., 106, 7183-7192, 2001.

Wenzel, A., Kalthoff, N., and Horlacher, V.: On the profiles of wind velocity in the roughness sublayer above a coniferous forest, Bound.-Lay. Meteorol., 84, 219-230, 1997.

Wyszogrodzki, A. A., Liu, Y., Jacobs, N., Childs, P., Zhang, Y., Roux, G., and Warner, T. T.: Analysis of the surface temperature and wind forecast errors of the NCAR-AirDat operational CONUS 4-km WRF forecasting system, Meteorol. Atmos. Phys., 122, 125-143, 2013.

Zahumenský, I.: Guidelines on quality control procedures for data from automatic weather stations. World Meteorological Organization, Switzerland, 2004.

Zhan, E., Dias, N. L., Araújo, A., Sá, L. D. A., Sörgel, M., Trebs, I., Wolff, S., and Manzi, A.: Scalar turbulent behavior in the roughness sublayer of an Amazonian forest, Atmos. Chem. Phys., 16, 11349-11366, 2016.

Table 1: Idealized boundary condition for the one-dimensional offline simulation. Constant z_0 is used only in the CTL experiment.

Variable	Value	Variable	Value
h	18 m	S_m	0.25 m^3 m^{-3}
LAI	4 m^2 m^{-2}	$T(z_r)$	300 K
Land-use category	Mixed forest	T_{sk}	303 K
L_c	18 m	$u(z_r)$	3 m s^{-1}
$p(z_r)$	1000 hPa	u_*	0.5 m s^{-1}
$q(z_r)$	9.3·10 kg kg^{-3}	z/L	−10–10
SW	800 W m^{-2}	z_0	0.25 m

Table 2.: Statistics of the 10 m wind speed, 2 m temperature, and rain rate. The top statistics are presented in bold.

	rCTL	rRSL
10 m wind speed		
Mean bias (m s^{-1})	2.4	**1.0**
Root–mean–square error (m s^{-1})	3.1	**1.8**
2 m temperature		
Mean bias (K)	**−0.92**	−1.16
Root–mean–square error (K)	2.74	**2.67**
Rain rate		
Mean bias (mm h^{-1})	−0.018	**−0.018**
Root–mean–square error (mm h^{-1})	0.194	**0.187**
Pattern correlation	0.972	**0.978**

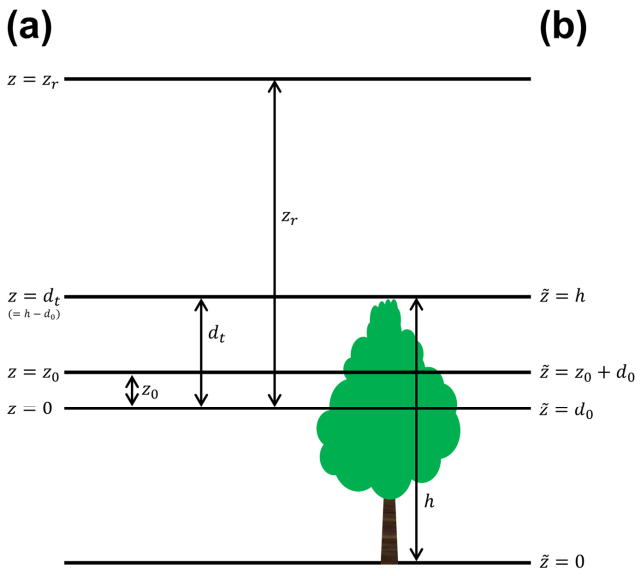

Formatted: English (United States)

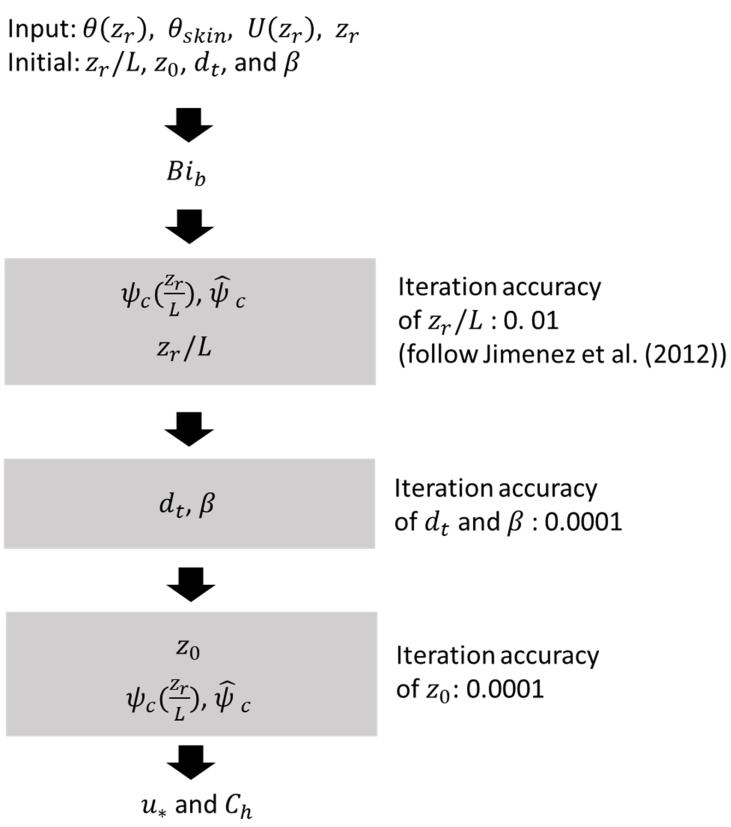

~~Figure 1~~Figure 1: The schematic diagram to describe the vertical coordinate systems used in this study. (a) vertical Coordinates of the YSL schemes (z) is defined as the distance from the conventional zero-plane displacement height (d_0) and (b) the convectional coordinate ($\tilde{z}$) is defined as the distance from terrain surface. Here z_0, d_t, h, and z_r are roughness length, the redefined zero-plane displacement height in Harman and Finnigan (2007), canopy height, and the lowest model layer in the conventional coordinate, respectively.

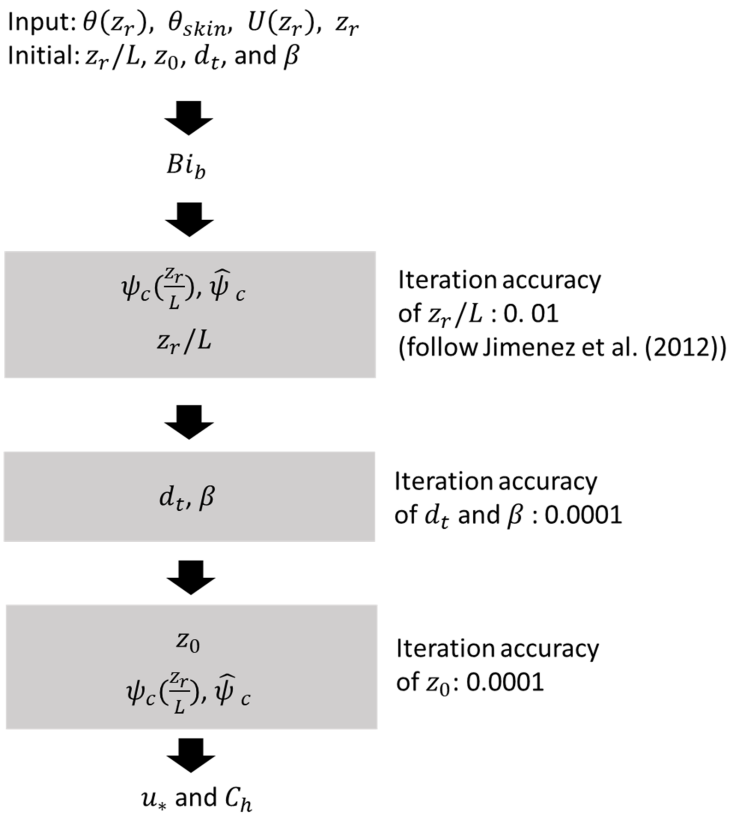

Figure 2: Flow diagram of the RSL parameterization. The gray boxes indicate the iteration module.

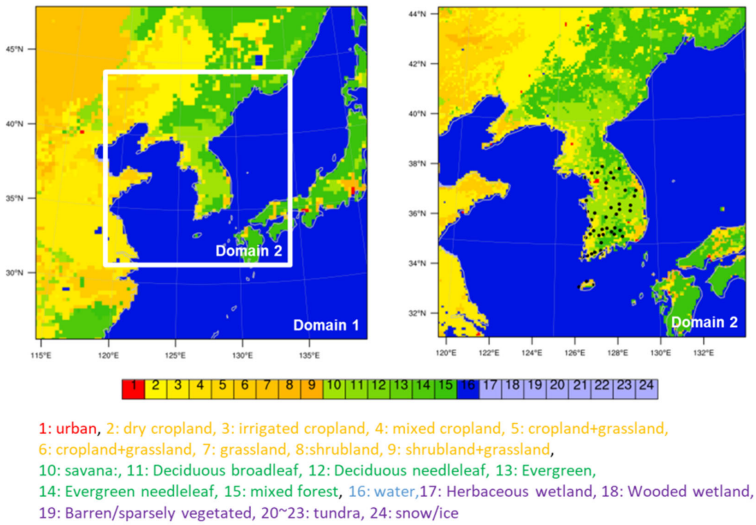

Figure ~~2.~~3: Domains and land-use category (USGS) of the real case simulation. Black circles denote the automatic synoptic observing system in Korea used for the model validation.

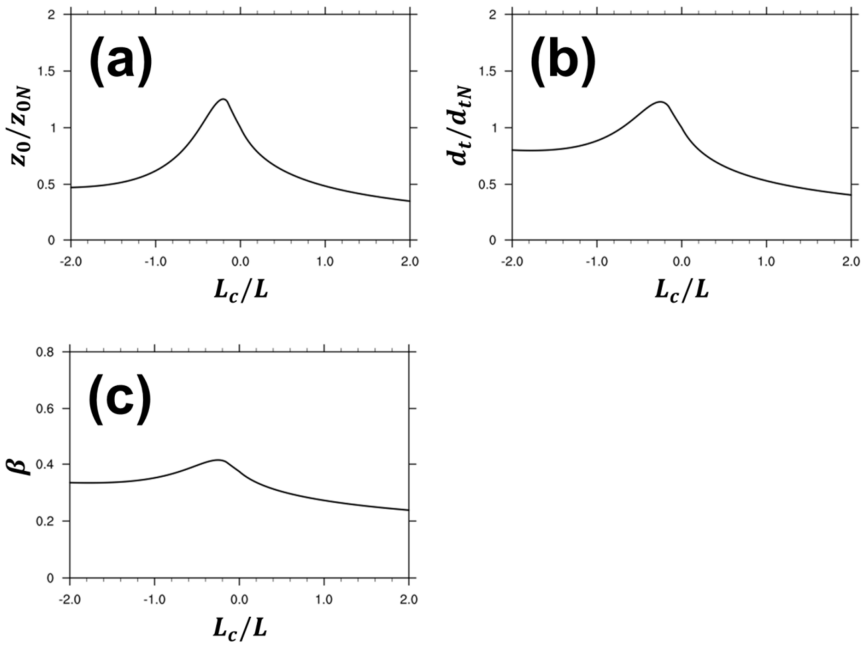

375

Figure ~~3.~~4: Roughness length (a), redefined displacement height (b), and β (c) ~~normalized by its values in a neutral condition~~ at a given normalized stability (L_c/L) from the ~~offline~~offRSL simulation with the YSL scheme. Roughness length and redefined displacement height are normalized by their values in a neutral condition (z_{0N} and d_{tN}), respectively.

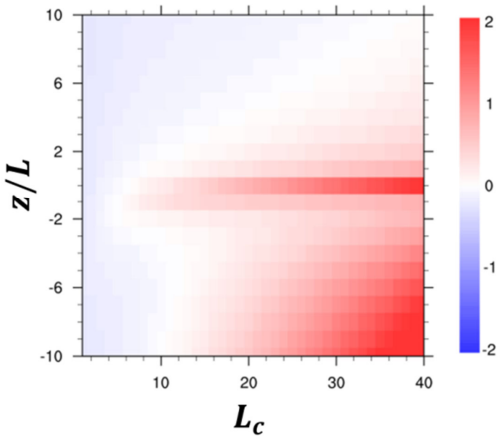

Figure 4.5: Roughness length difference (m) between offCTL and offRSL (offRSL − offCTL) at given atmospheric stability (z/L) and penetration depth (L_c).

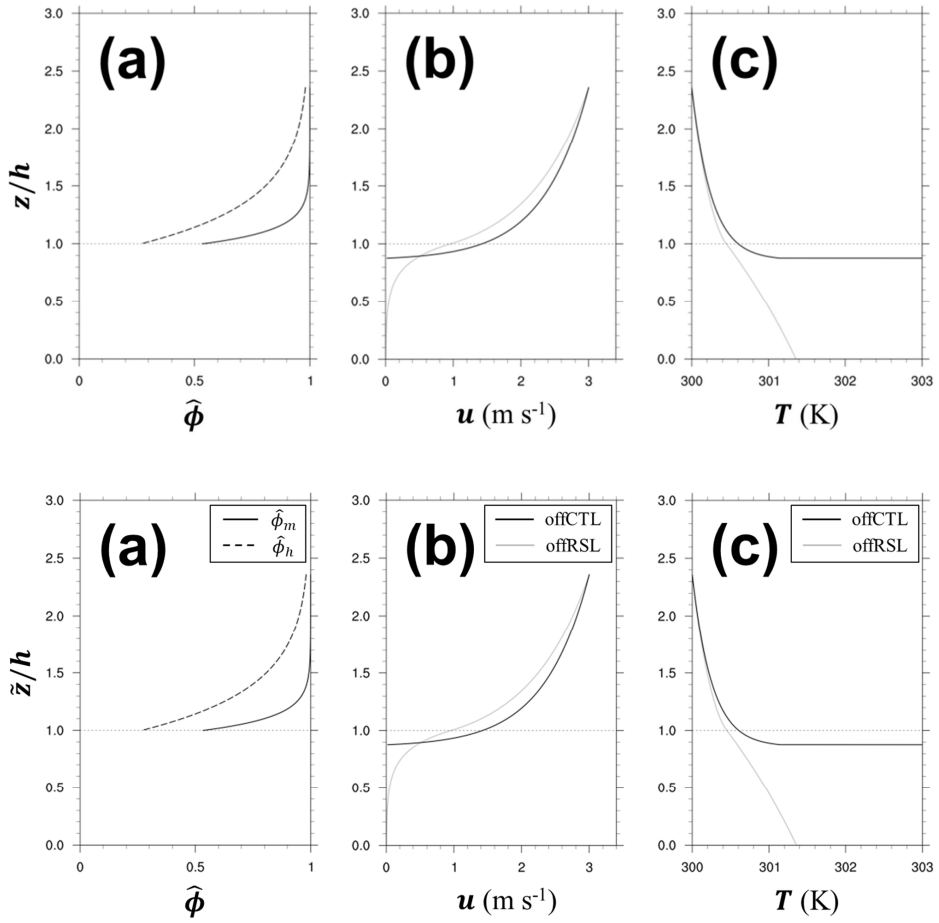

385

Figure ~~5.~~6: (a) Profiles of the RSL function for momentum ($\hat{\phi}_m$, solid line) and heat ($\hat{\phi}_h$, dashed line), (b) wind speed (m s^{-1}), and (c) temperature (K) at a neutral condition from offCTL (black) and offRSL (gray). The height ~~(z)~~of conventional coordinate system ($\tilde{z}$) is normalized by the canopy height (h).

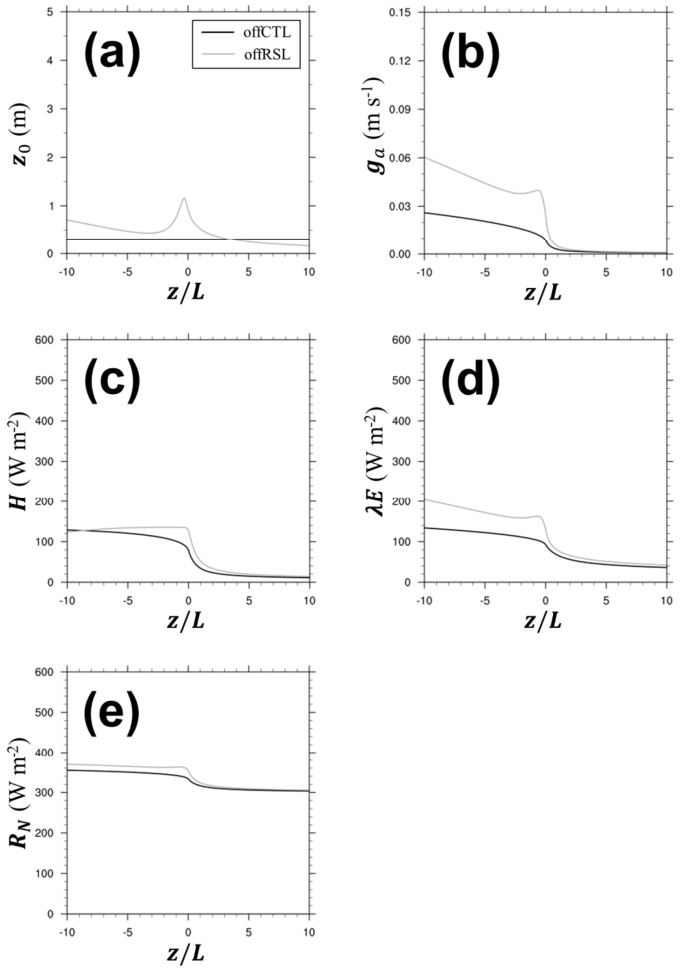

390

Figure 6.7: (a) Roughness length (m), (b) aerodynamic conductance (m s^{-1}), (c) sensible heat flux (W m^{-2}), (d) latent heat flux (W m^{-2}), and (e) net radiation (W m^{-2}) at a given atmospheric stability (z/L). The black lines denote offCTL, while the gray lines denote offRSL

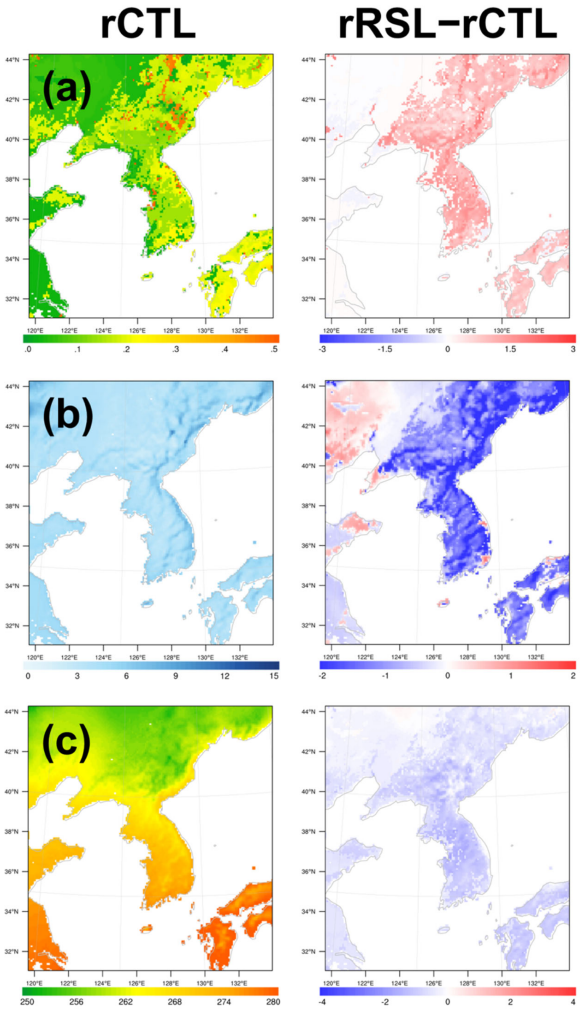

Figure ~~7.~~8: (a) Roughness length (m), (b) 10 m wind speed (m s^{-1}), and (c) daytime 2 m temperature (K) of the (left) rCTL experiment and (right) the difference (rRSL − rCTL). The results are averaged over a period of one month and masked out over the ocean.

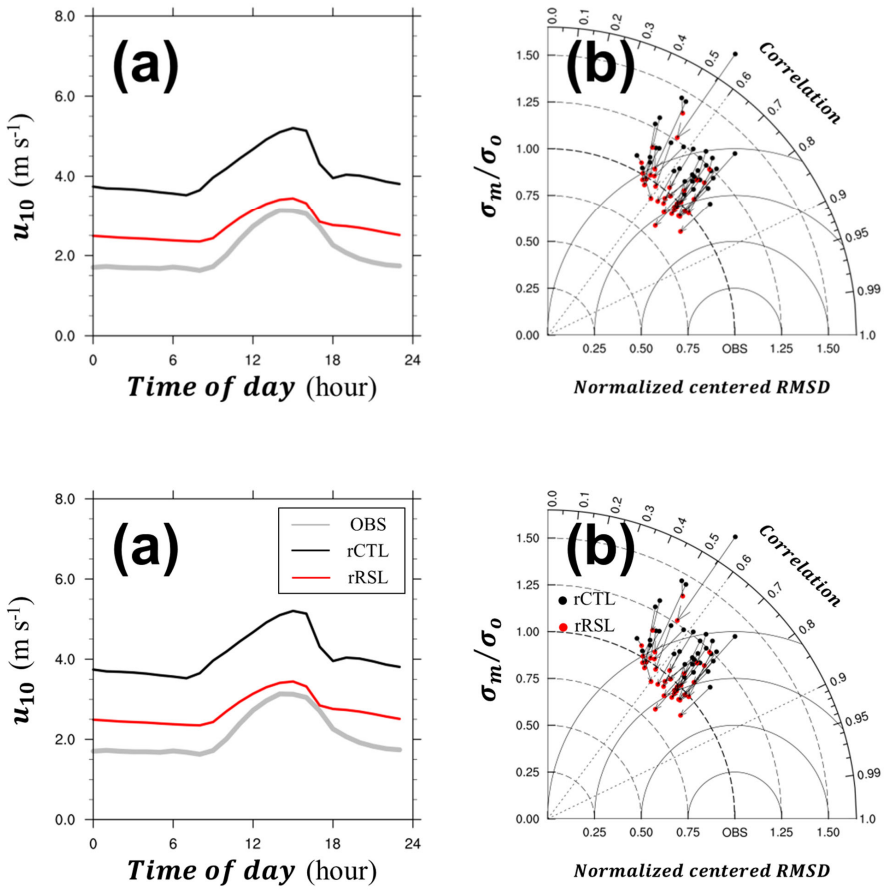

Figure 8-9: (a) One month mean diurnal variation of 10 m wind speed and (b) the Taylor diagram showing the correlation coefficient, normalized centered root–mean–square differences (RMSD), and standard deviations of the models (σ_m) normalized by that of observation (σ_o) from observation (gray), rCTL experiment (black), and rRSL experiment (red). The vectors indicate the changes of the statistics from rCTL to rRSL. The arrows indicate those from rCTL to rRSL. Every vector shows the movement toward the observation, thereby suggesting the model improvement.

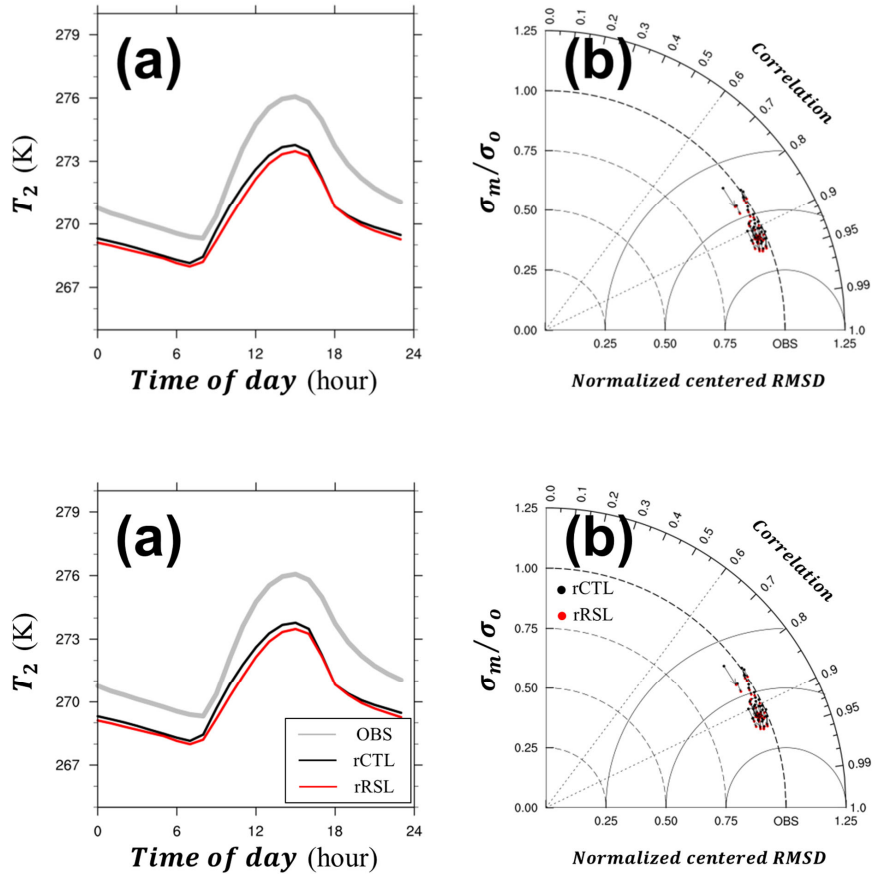

Figure 9.10: Same as in Fig. 89, but for the 2 m temperature.

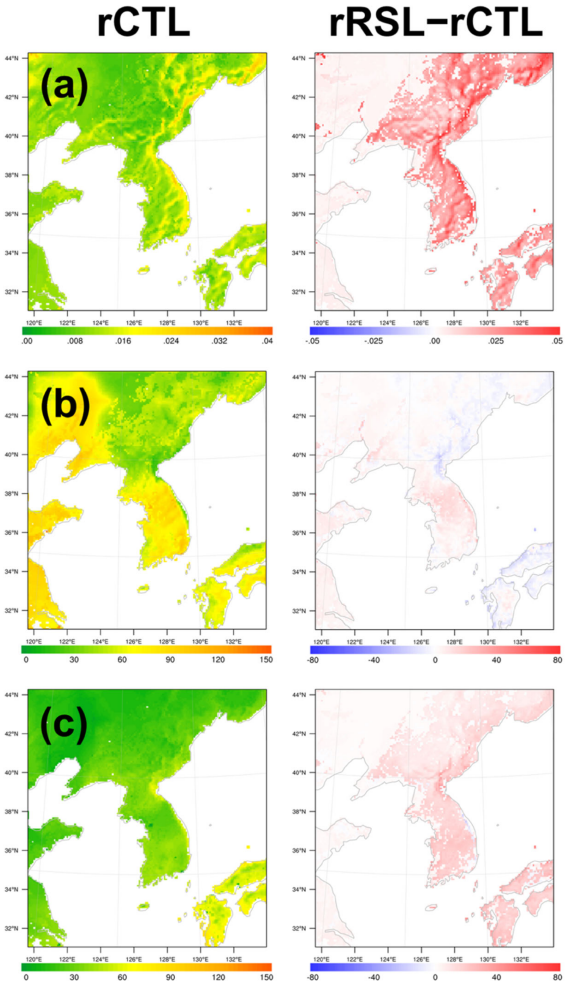

Figure ~~10.~~11: (a) Aerodynamic conductance (m s^{-1}), (b) daytime sensible heat flux (W m^{-2}), and (c) daytime latent heat flux (W m^{-2}) of the (left) rCTL experiment and (right) the difference (rRSL − rCTL). The results are averaged over a period of one month and masked out over the ocean.

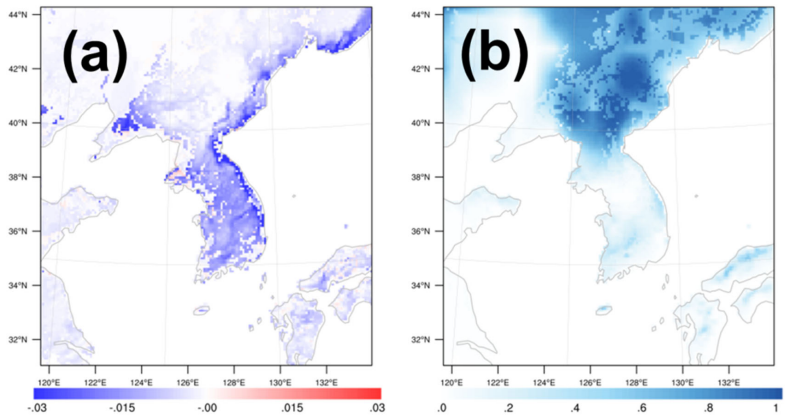

415

Figure ~~11.~~12: (a) Difference of the soil moisture ($m^3\ m^{-3}$) (rRSL − rCTL) and (b) snow cover (%) of rCTL. The results are averaged over a period of one month and masked out over the ocean.

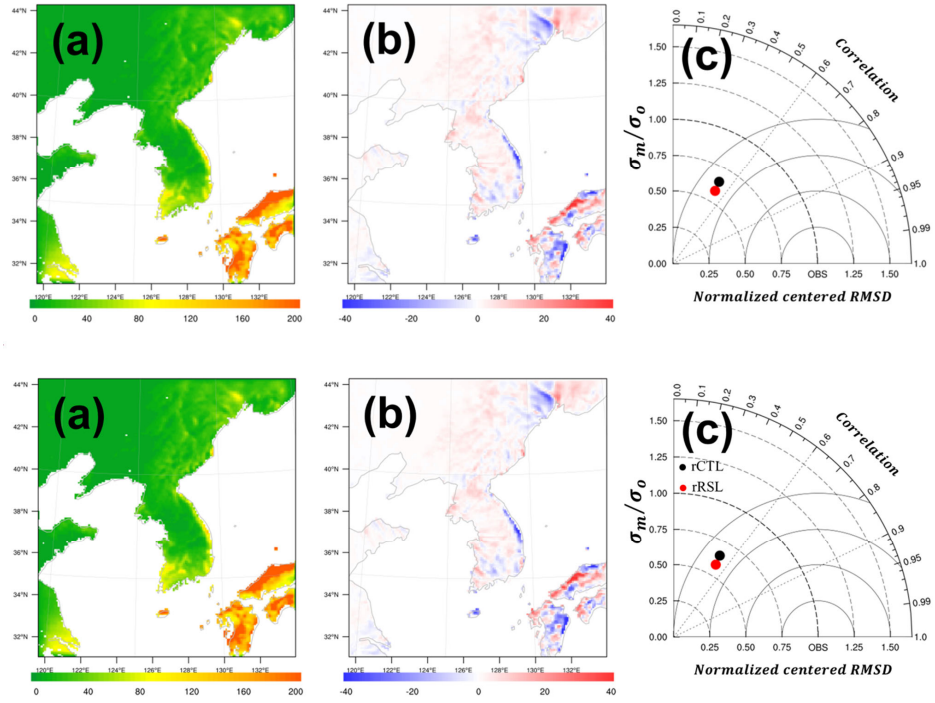

Figure ~~12.~~13: (a) One month accumulated precipitation of the rCTL experiment (mm) and (b) difference (rRSL − rCTL). (c) Taylor diagram showing the correlation coefficient, normalized centered root–mean–square difference (RMSD), and the standard deviations of models (σ_m) normalized by that of the observation (σ_o) and from the rain rate (mm h^{-1}) of the rCTL experiment (black) and the rRSL experiment (red) during one month at 656 rain gauges.